Six Pole type Hybrid Magnetic Bearing for Turbo-Machinery

Yohji OKADA*, Masaki TOUNO*, Ken-Ichi MATSUDA*, Ryou KONDO* and Takashi TODAKA**

* Dept. of Mechanical Engineering, Ibaraki University
4-12-1 Nakanarusawa, Hitachi, Ibaraki-pref. 316-8511, Japan
E-mail: yohji.okada.spam@vc.ibaraki.ac.jp

** Dept. of Electrical and Electronic Engineering, Oita University
700 Dannoharu, Oita, Oita-pref. 870-1192, Japan

Abstract

New six pole type hybrid magnetic bearing is introduced. It is intended to apply to high speed turbo-machinery. Traditionally turbo-machinery uses standard electro-magnet (EM) type active magnetic bearing (AMB) which requires PWM power amplifiers. Recently turbo manufacturer wants to develop their own magnetic bearing. Sometimes they are not accustomed with developing standard EM type magnetic bearings. The proposed magnetic bearing uses bias Permanent Magnet (PM), hence it is easily manufactured. The developed magnetic bearing also has good characteristics due to six directional control pole compared with the standard four directional control one.

Key words : Magnetic bearing, Actuator, Rotating machinery, Digital control, Mechatronics

1. Introduction

New six pole type hybrid magnetic bearing is introduced. It is intended to apply to high speed turbo-machinery. Traditionally turbo-machinery uses standard electro-magnet (EM) type active magnetic bearing (AMB) which requires Pulse Width Modulated (PWM) power amplifiers (Schweitzer and Maslen, 2009), (MECOS AG., 2016). Recently turbo-manufacturer wants to develop their own magnetic bearing (Filatov and Hawkins, 2014). Sometimes they are not accustomed with developing standard EM type magnetic bearings.

The proposed radial magnetic bearing has two stator yokes; front one is polarized S while back one is polarized N. Ring type PM is sandwiched between two stator yokes. Neodymium PM has been improved which can use over 150^oC. Both stator yokes have three salient poles with control windings, the opposite pairs of which are connected series and controlled by three power amplifiers. Thanks to strong bias flux produced by rare earth PM, the force factor is high (Kakihara, et. al., 2006), (Kodama, et. al., 2006), (Martin, et. al., 2004), (Miyazawa, et. al., 2009), (Okada, et. al., 2011). Hence the proposed AMB can be driven by three standard bipolar linear power amplifiers.

First, the operating principle of the proposed AMB is introduced compared with the traditional electro-magnet type AMB which are shown in Figs. 1 to 4. The control difficulty of the traditional one is explained which requires push-pull operating unipolar PWM power amplifiers. Then the analytical model of the proposed AMB is introduced which is

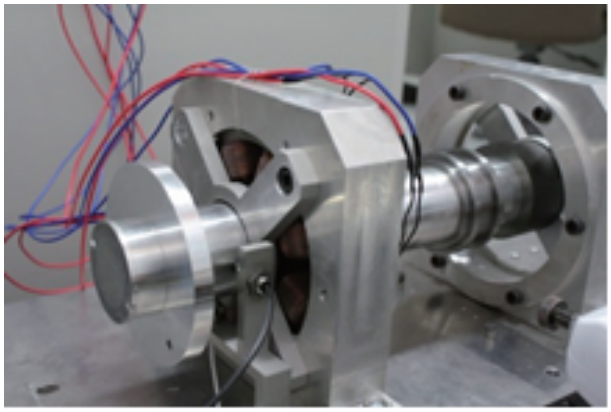

Fig. 1 Experimental setup of electro-magnet (EM) type AMB

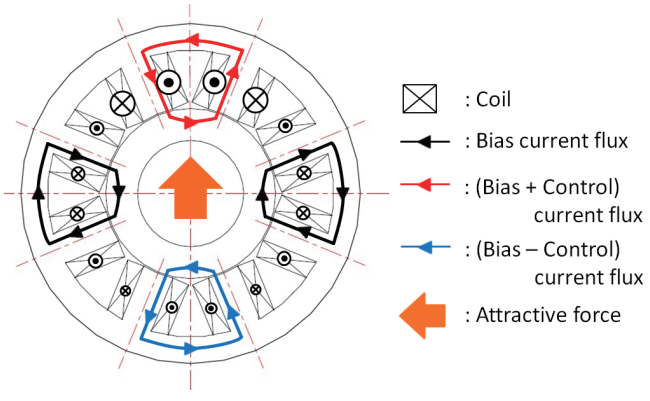

Fig. 2 Principle of electro-magnet (EM) type AMB

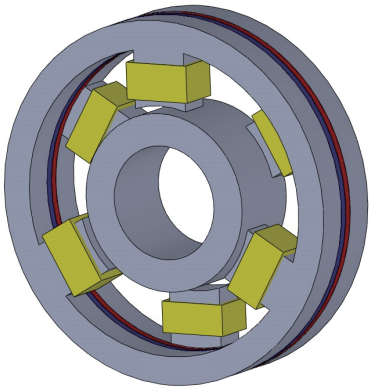

Fig. 3 Scheme of proposed hybrid (HB) type AMB

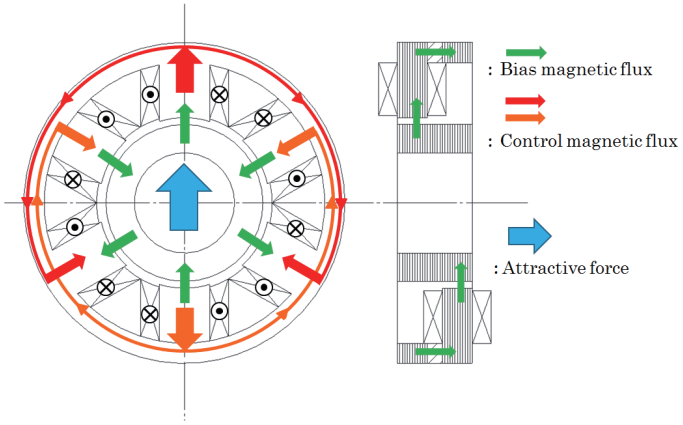

Fig. 4 Principle of proposed hybrid (HB) type AMB

analyzed and designed through the commercial finite element method (FEM) magnetic field analysis.

Then, the experimental setup is fabricated. The levitation control test is carried out which shows stable levitation and rotation of the proposed AMB with the standard PID controller.

2. Problem of electro-magnet type magnetic bearing

Electro-magnet type magnetic bearing is widely used to support the rotor of turbo machinery. The principle is shown in Fig. 2. This type AMB has merits of simple structure and big supporting force compared with its size. Also the air gap can be narrow to seal fluid between the AMB. However it requires special PWM power amplifier to control the differential attractive force,

$$F_m = \frac{(B_b + B_c)^2 S - (B_b - B_c)^2 S}{2\mu_o} = \frac{2B_b B_c S}{\mu_o} \tag{1}$$

where F_m is the control force, B_b is the bias flux, B_c is the control flux, S is the flux area and μ_o is the permeability of free space.

The upper and lower fluxes $(B_b + B_c)$, $(B_b - B_c)$ should be controlled by the differential type unipolar PWM power amplifier which is not easily manufactured.

3. Principle of the proposed magnetic bearing

In this paper a new hybrid type AMB is developed which can be driven by commercially available power amplifiers. Scheme and the operating principle of which are shown in Figs. 3 and 4, respectively. Two stator yokes have three salient poles with control windings. Strong permanent magnet (PM) is sandwiched by two stator yokes; the front yoke is polarized S while the back one is polarized N. The bias fluxes are flown as shown by the green arrows. The opposite coils are connected series, and three coil pairs are driven by three phase power amplifiers. The control fluxes in the front core are shown by the red arrows while those in back core are shown by the orange arrows. The upper fluxes are strengthened while the lower fluxes are weakened causing upward force as shown by the blue arrow. Similar control can be applied to the horizontal direction. Hence the radial two directions can be controlled actively.

In this paper pole number six is adopted. Two directional forces can be controlled by four pole AMB. But the space efficiency is not good because the circular back yoke and rotor yoke are not well fit with four poles. Eight pole is well fit with such circular rotor, but it requires four power amplifiers. For this reason we choose six pole magnetic bearing system.

4. Finite element analysis and design

The proposed magnetic bearing is analyzed and designed through the commercial finite element method (FEM) ANSYS. The model and the main parameters are shown in Fig. 5 and Table 1, respectively. The outer diameter of ϕ128, the stack thickness of 30 mm and the rotor shaft diameter of ϕ40 are determined as the same values of the previously

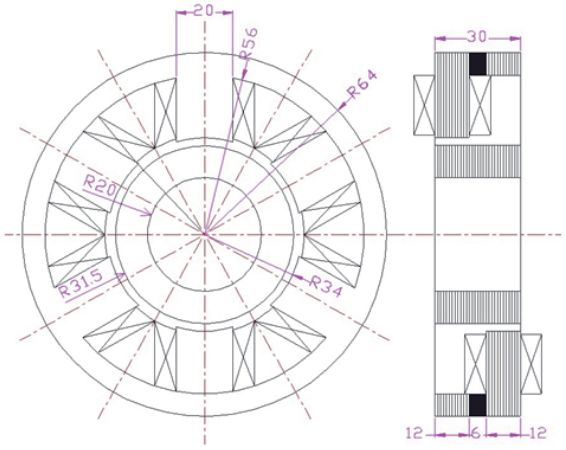

Fig. 5 Analytical model of proposed AMB

Table 1 Main parameters of analysis

Item	Value or Material
Air gap [mm]	2.5 ⇒ 1.5
Coil turns [turn/pole]	250
Core material	Laminated silicon steel (35A300)
PM material	N41TU (Shin-Etsu Magnetic Inc.)

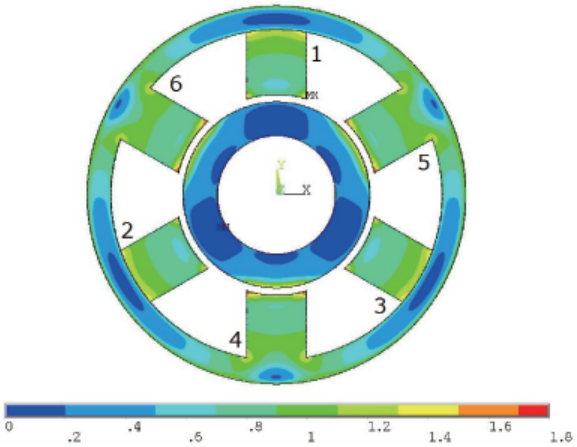

Fig. 6 Bias flux density with air gap of 2.5 mm

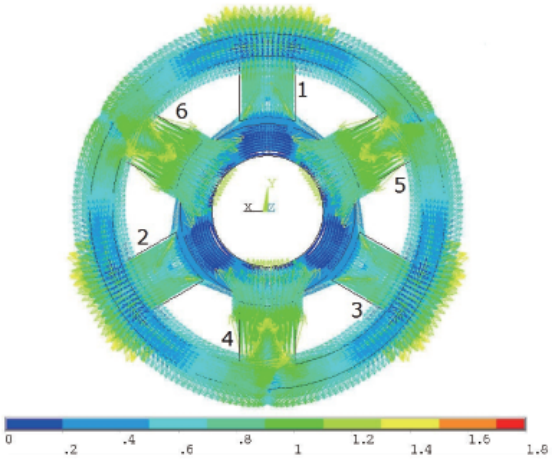

Fig. 7 Bias flux vector with air gap of 2.5 mm

designed electro-magnet type AMB which is shown in Figs. 1 and 2. The other parameters are determined through the analysis as shown in Table 1.

First, we used the air gap 2.5 mm because the attractive force produced by PM is very strong. Fiber reinforced plastics (FRP) pipe with thickness of 2 mm is used inside the stator which prevents the stack of rotor (Fujihira Co., Ltd., 2016). After the first trial, the manufacturer succeed to produce FRP pipe with the thickness of 1 mm. Hence we extend only the rotor outer radius of 1 mm, this means that the air gap is reduced to 1.5 mm.

4.1. Bias Flux density distribution

First, the bias flux density distribution is analyzed. The results of air gap 2.5 mm are shown in Figs. 6 and 7. Figure 6 shows the bias flux density while Fig. 7 is the bias flux vectors. The bias flux is well formed as shown in Fig. 6. As expected the front yoke vectors of poles numbered 1, 2 and 3 direct outside, while the back yoke vectors of poles numbered 4, 5 and 6 direct inside as shown in Fig. 7. The bias flux density distributions of the air gaps of 2.5 mm and 1.5 mm are shown by the red line and blue line in Fig. 8, respectively. The maximum flux density is about 0.41 T of the air gap 2.5 mm and 0.51 T of the air gap 1.5 mm. They are enough high compared with the wide air gaps. These graphs include the experimental results mentioned later.

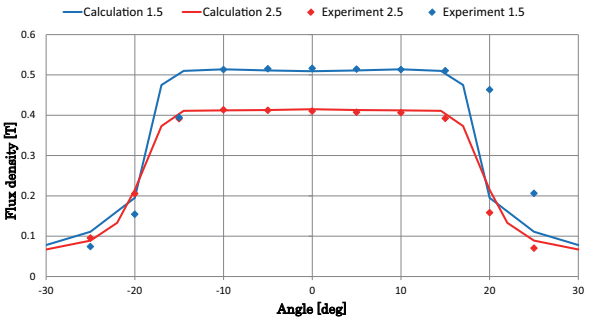

Fig. 8 Comparison of bias flux density distributions

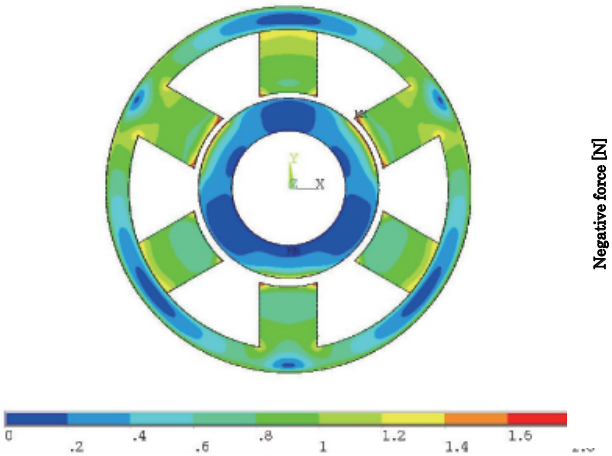

Fig. 9 Flux density distribution (0.5 mm displacement), air gap of 2.5 mm

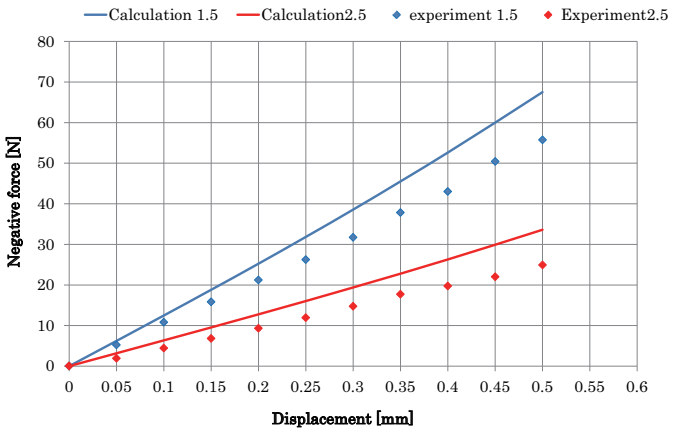

Fig. 10 Negative forces with air gap of 2.5 mm and 1.5 mm

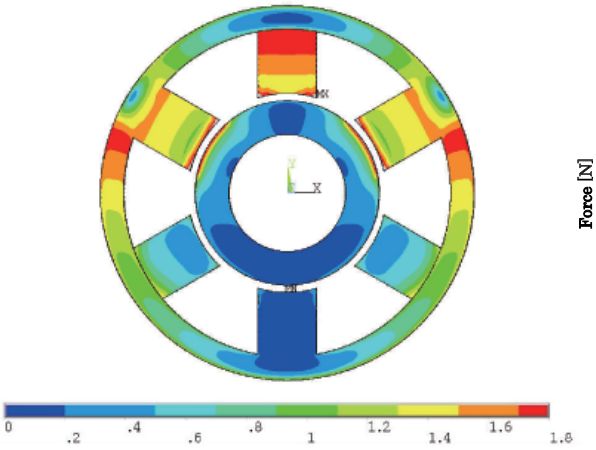

Fig. 11 Flux density distribution (current=3 A), air gap of 2.5 mm

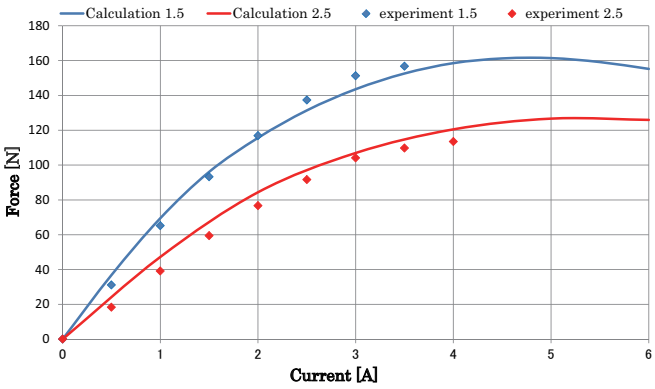

Fig. 12 Control forces with air gap of 2.5 mm and 1.5 mm

4.2. Negative force

The negative force is analyzed by displacing the rotor upward 0 to 0.5 mm from the center of the stator and calculating the resulting magnetic forces. The flux density at 0.5 mm displaced rotor upward with the air gap 2.5 mm is shown in Fig. 9. The upper flux is strengthened while the lower flux is weakened. The resulting negative forces are shown by the red line of air gap 2.5 mm and those are shown by blue line of air gap 1.5 mm in Fig. 10, respectively. The negative force factors are 66 kN/m with air gap 2.5 mm and 134 kN/m with air gap 1.5 mm, respectively.

4.3. Control force

The control force is calculated by giving the three phase currents (I_u, I_v, I_w) which are calculated by converting from the two phase current as

$$\begin{bmatrix} I_u \\ I_v \\ I_w \end{bmatrix} = \sqrt{\frac{2}{3}} \begin{bmatrix} 1 & 0 \\ -0.5 & 0.866 \\ -0.5 & -0.866 \end{bmatrix} \begin{bmatrix} I_y \\ I_x \end{bmatrix} \tag{2}$$

during the rotor kept at the center of stator. The flux density by giving the y-directional current of 3 A ($I_y = 3$) for air gap 2.5 mm is shown in Fig. 11. The upper pole flux is almost saturation level, while the lower pole flux is almost zero.

The resulting control forces are shown by the red line for air gap 2.5 mm and the blue line for air gap 1.5 mm in Fig. 12, respectively. The force factors of 45 N/A for air gap 2.5 mm and 70 N/A for air gap 1.5 mm are calculated as shown in Fig. 12. They are considered enough high compared with the negative force factors.

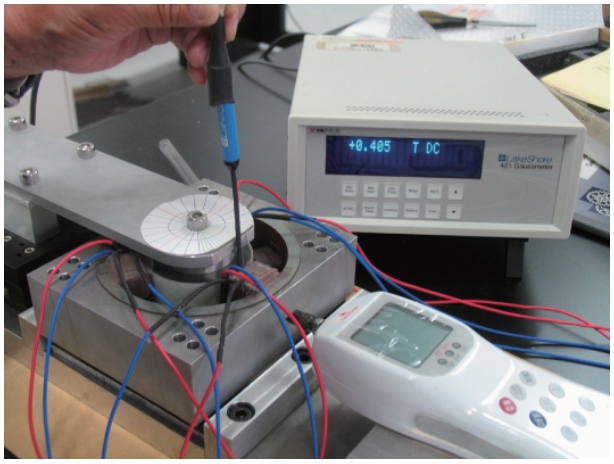

Fig. 13 Bias flux density measurement with air gap of 2.5 mm

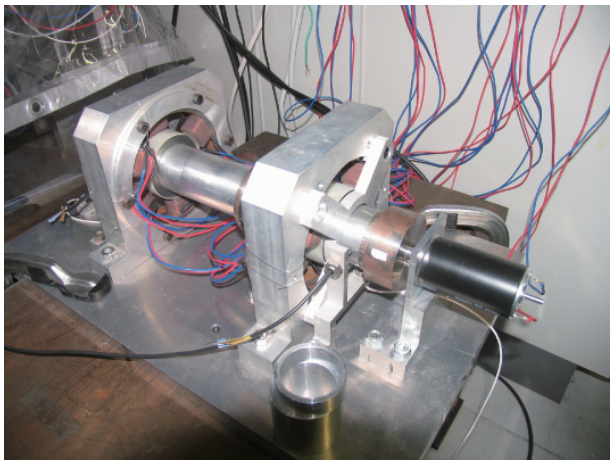

Fig. 14 Photo of levitation control

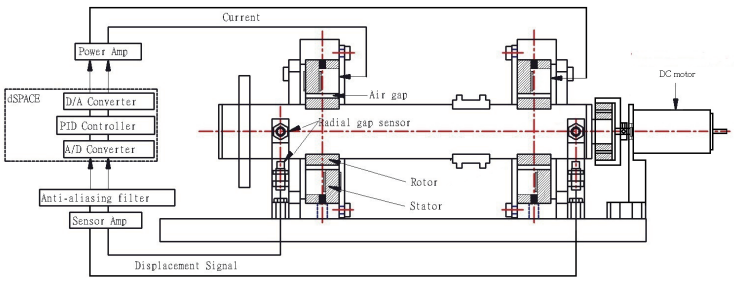

Fig. 15 Scheme of rotor and control system

Table 2 Control gains

	Free side		Motor side	
	x-dir.	y-dir.	x-dir.	y-dir.
P gain K_p [A/mm]	4.0	4.0	7.0	10.0
I gain K_i [A/s mm]	0.5	0.5	1.0	1.0
D gain K_d [A s/mm]	0.004	0.004	0.007	0.009

5. Experiment

The experimental setup is fabricated and tested. First the static characteristics are measured and compared with the analytical results. Then the levitated response tests are carried out. Finally the levitated rotation is tested.

5.1. Bias flux and force characteristics

Bias flux in air gap is measured by centering the rotor and inserting the Gauss meter probe (Lake Shore 421, probe: MFT-3E03-VH) in air gap as shown in Fig. 13. The results are shown by the red dots (air gap 2.5 mm) and blue dots (air gap 1.5 mm) in Fig. 8. The measured flux values are well agreed with the calculated values except both sides of stator pole edges. This might be due to the non-accurate inserting angle by hand on the angle scale.

After pull out the Gauss meter probe, negative forces are measured by moving the rotor position by micro stage and measuring the resulting force by force meter (Aikoh RX-100). The results are shown by red dots (air gap 2.5 mm) and blue dots (air gap 1.5 mm) as shown in Fig. 10. The measured results are lower than the calculated values. The negative force factor of air gap 2.5 mm is about 50 kN/m, while that of air gap 1.5 mm is about 110 kN/m.

Also control force is measured by giving the driving current to y-direction and measuring the centered rotor force. The resulting forces are shown by the red dots (air gap 2.5 mm) and blue dots (air gap 1.5 mm) in Fig. 12. In this case the measured values are relatively close to the calculated values. The forces are almost linear up to 2 A. Over 3 A control forces saturate due to the nonlinear property of silicon steel sheet.

5.2. Levitation control

The levitation test is carried out as shown in Fig. 14. Both of the air gap 2.5 and 1.5 mm are tested, but the better results are obtained in the case of 1.5 mm air gap. Hence only the results of air gap 1.5 are reported here. Scheme of levitation test and control system are shown in Fig. 15. Four radial directions are actively controlled, while the axial direction relies on passive stability. The radial displacements are measured by eddy current probes (x-directions: Keyence EX-502, y-directions: Shinkawa VCD-020) and put into dSPACE (DS-1104) through 3rd order anti-aliasing filter, the corner frequency of which is 5 kHz. The control algorism used is local PID controller, the gains are listed in Table 2. The control gains of the free side is lower than those of motor side, because the magnetic coupling used is strong and we need

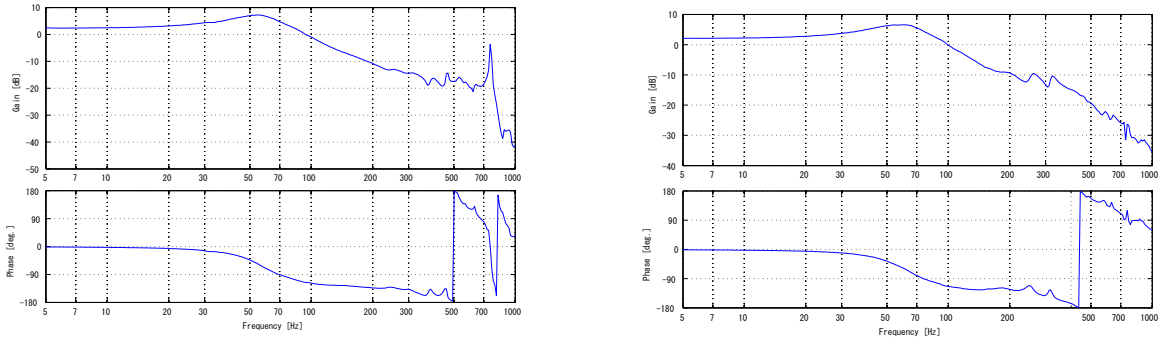

Fig. 16 Frequency response of free side (left:x-direction (horizontal), right:y-direction(vertical))

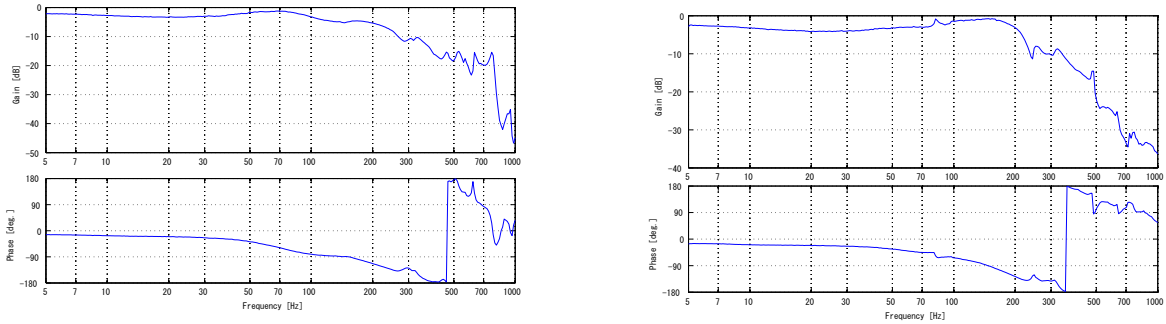

Fig. 17 Frequency response of motor side (left:x-direction (horizontal), right:y-direction(vertical))

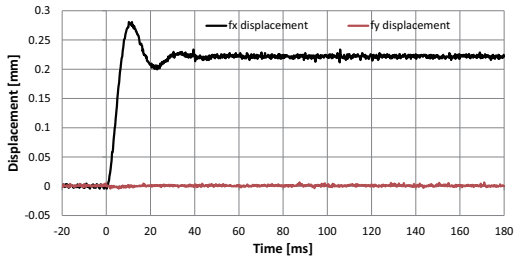

Fig. 18 Step response of x-direc. excitation and x-y responses

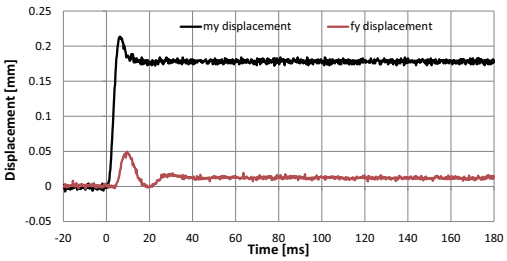

Fig. 19 Step response of motor-side excitation and m-f responses

high gains. The sampling interval τ used is 0.05 ms. The calculated demand signals are put out to analog power amplifiers (APEX PA-12A) via D/A converter.

Thanks to the high bias flux produced by PMs, the levitation is very stable. This is considered due to the good linearity and accurate control angle of the six directional control pole mentioned later. First the frequency response test is carried out by giving the sinusoidal signal of 20 μm magnitude and the frequency range from 5 Hz to 1 kHz, and recording the resulting displacement. The frequency response analyzer (NF Corp. FRA-5095) is used. The results are shown in Figs. 16 and 17. All the responses are well reduced by the PID controller. The free side peaks are about 7 dB at 55 Hz. On the contrary the motor side responses are complicated.

5.3. Step response

The step response tests are carried out, two examples are shown in Figs. 18 and 19. Figure 18 shows the responses of free side x, y-directional displacements when the x-direction is excited by 0.2 mm step. There is no interference between x and y directions, but the response of x direction is about 0.22 mm. Figure 19 is the response of motor side and free side y-directional responses when motor side is excited by 0.2 mm step. In this case the motor side displacement is 0.18 mm, while the free side displacement is 0.02 mm. This means that there are some interference between the motor and free sides. This may be caused by strong attractive force of the magnetic coupling which is installed to give rotating torque to the rotor without physical contact.

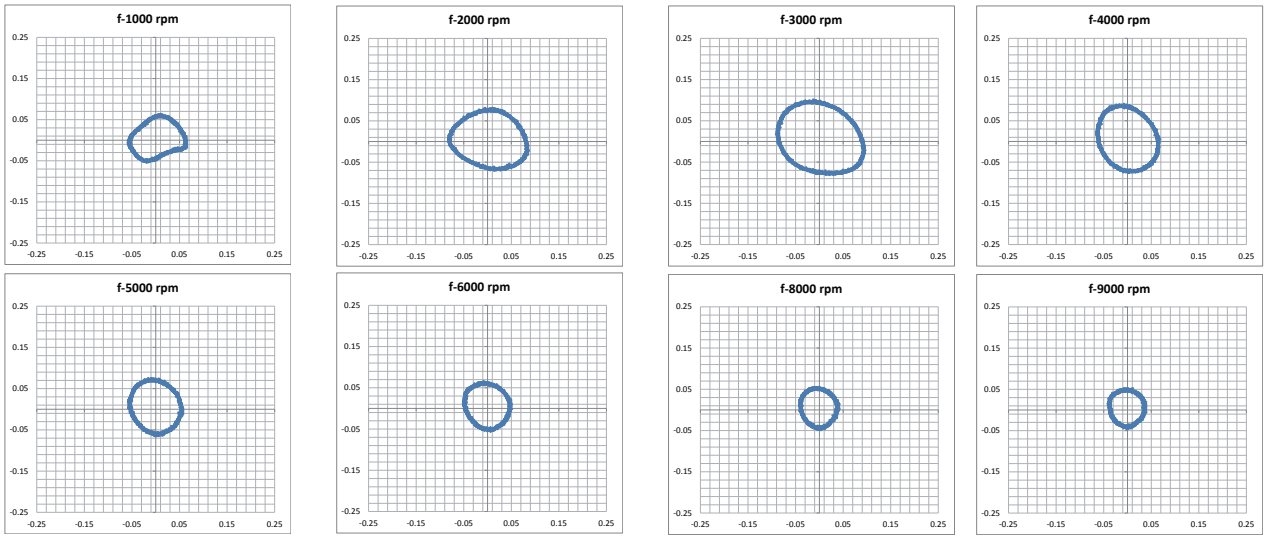

Fig. 20 Orbital trajectories of the free side (1000 rpm to 9000 rpm)

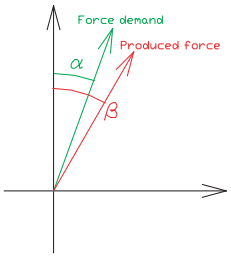

Fig. 21 Angular error

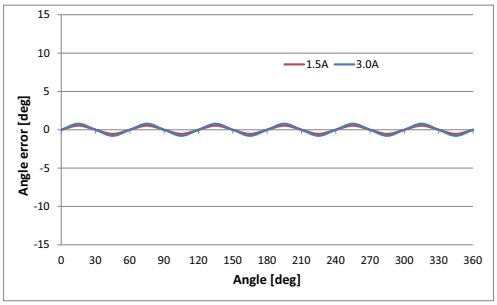

Fig. 22 HB AMB angular error of air gap 1.5 mm

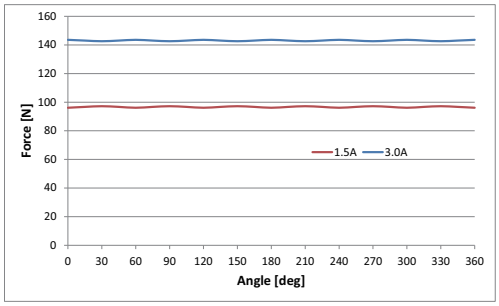

Fig. 23 HB AMB force magnitude of air gap 1.5 mm

5.4. Rotating test

Rotating test is carried out by driving the rotor through magnetic coupling by DC motor. The driving motor (maxon 148877) is installed in the right end of Figs. 14 and 15. The orbital trajectories are measured by rotating the rotor from 1000 to 9000 rpm. The resulting trajectories of free side are shown in Fig. 20 except the case of 7000 rpm. All the trajectories are within ±120 μm. According to the rotating speed the vibration is increased up to 3000 rpm. Over which the vibration is decreased and it becomes about ±50 μm at 9000 rpm. This is due to the resonant frequency of 55 Hz (3300 rpm).

6. Angular force analysis

In this paper angular error analysis is carried out which is schematically shown in Fig. 21. In radial plane of magnetic bearing, the demand force has angle of α as shown by the green arrow and the produced force has angle β as shown by the red arrow. Then the angle difference $\beta - \alpha$ is defined as the angular error.

6.1. Angular error of proposed AMB

First, we analyze the angular error and produced force of the proposed HB type magnetic bearing of air gap 1.5 mm from α = 0 to 360 deg. The results of angular errors are shown in Figs. 22 and the produced forces are in Fig. 23. The angular error is very small about 1.5 deg. when the driving current is 3 A. Good angular accuracy might be the results of six directional control directions, but the produced force is relatively weak compared with the traditional electro-magnet type AMB.

6.2. Angular error of electro-magnet type AMB

Next, the traditional electro-magnet type magnetic bearing is analyzed. Analytical model is shown in Fig. 24. This model is the same magnetic bearing of the previous photo (in Fig.1) and the explaining picture (in Fig. 2). The analytical

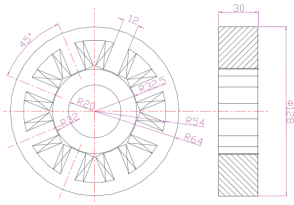

Fig. 24 Model of EM AMB

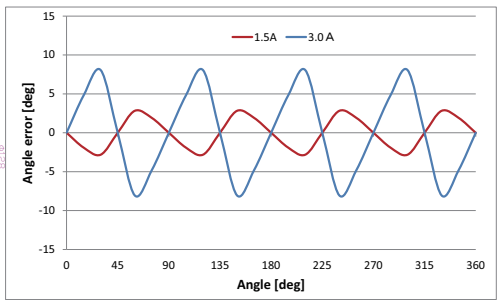

Fig. 25 EM AMB angle error of air gap 0.5 mm

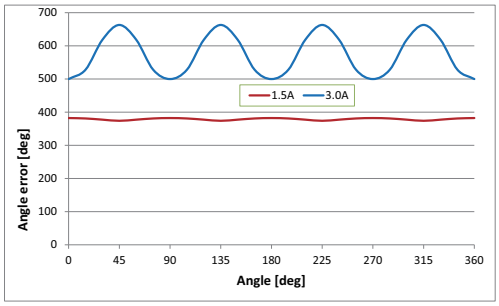

Fig. 26 HB AMB force magnitude of air gap 0.5 mm

results of angular error are shown in Fig. 25, which shows bigger angular error up to 8 deg. at 3 A, compared with the proposed one. This might be due to the small number of four control directions of EM type AMB. However the produced force is much stronger, over 500 N at 3 A than the previous case. This is considered as a strong merit of EM type AMB, but the analyzed EM type magnetic bearing has the air gap of 0.5 mm. If we can develop the proposed AMB with the narrow air gap of 0.5 mm, the maximum force may be improved.

7. Concluding remarks

New six pole hybrid type active magnetic bearing is developed which is planned to apply to high speed turbo machinery. Compared to the traditional electro-magnet type magnetic bearing the proposed one is easily developed and controlled. The levitation stability is very good. This is mainly due to the high bias flux produced by the bias permanent magnet which can produce strong force factor and good linearity. Also six directional control poles can produce accurate angular force than the traditional one. The experimental setup is designed and fabricated. The results show good dynamic characteristics supported by the proposed magnetic bearing with the standard PID controller.

Acknowledgement

This research is carried out at Ibaraki University under the consigned research foundation from Oita University.

References

Filatov, A. and Hawkins, L., Comparative Study of Axial/Radial Magnetic Bearing Arrangements for Turbocompressor Applications, Proc. of 14th International Symposium on Magnetic Bearings, (2014), pp.1-7, Linz, Austria.

Fujihira Co., Ltd., URL: http://www.fujihira-gr.co.jp/English/FRP

Kakihara, K., Otsuka, Y., Kurita, N., and Okada, Y., Development of Wide-Gap Hybrid Magnetic Bearing, CD-ROM Proc. of 8th Int. Conf. on Motion and Vibration Control, (2006), pp. 1-6, KAIST, Daejeon, Korea.

Kodama, S., et. al., Development of 5 DOF IPM Type Magnetic Bearing, CD-ROM Proc. of 8th Int. Conf. on Motion and Vibration Control, (2006), pp. 1-6, KAIST, Daejeon, Korea.

Martin, R., et. al., Development of A Low Cost Permanent Magnet Biased Bearing, CD-ROM Proc. of 9th Int. Symp. on Magnetic Bearings, (2004), pp. 1-6, Lexington, Kentucky, USA.

MECOS AG, URL: http://www.mecos.com/en/

Miyazawa, H., Okada, Y., Kondo, R., and Enokizono, M., Development of a Flux Concentrated PM Type Magnetic Bearings, Proc. of First Japan-Korea Joint Symposium on Dynamics and Control, (2009), pp. 183-186, Sapporo JAPAN.

Okada, Y., Miyazawa, H., Kondo, R., and Enokizono, M., Proposal of Flux Concentrated Radial and Axial Magnetic Bearings, Applied Electromagnetic Engineering, Edited by A. G. Mamalis, M. Enokizono, and A. Kladas, (2011), pp. 435-446, Trans Tech Publications LTD.

Schweitzer, G. and Maslen, E. H., ed., Magnetic Bearings, (2009), Springer.